Supplementary Materials

Characterization of Crz1-GFP.

Crz1-GFP abundance. Total abundance of Crz1-GFP remained approximately constant during the course of movies (Fig. S1). Thus the dynamic features we observe are based entirely on changes in localization.

Crz1-GFP is functional. We verified that the induction of target gene Cmk2 was similar between wild-type Crz1 and Crz1-mCherry strains, suggesting that the fluorescent protein fusion has minimal effect on the transcriptional activities of Crz1. Furthermore, in cells under calcium stress, addition of FK506, a Calcineurin inhibitor, suppresses Crz1-GFP localization bursts (Fig. S8), suggesting that the bursting behavior of Crz1localization depends on Calcineurin activity. Finally, we grew strains containing either (a) wild-type Crz1, (b) Crz1-GFP, or (c) ΔCrz1 on rich media with 0.8M NaCl and 4mM $MnCl_2$.[1] We found that Crz1-GFP complemented the growth defects found in Crz1Δ. These results suggest that growth and stress response are not compromised by the C-terminal GFP protein fusion.

Characterization of Crz1 bursts.

Distribution of burst number. The total number of bursts per single cell trace is not Poisson distributed (Fig. S4), as determined by the ratio of variance and mean. However, the two distributions of isolated bursts and burst clusters were each individually Poisson distributed, as shown by the close match of their cumulative distribution to that of the Poisson distribution and the low Kolmogorov-Smirnov (KS) scores, whereas the total bursts are less well-fit by Poisson distributions and have higher KS scores (Fig. S4).

Relative frequencies of burst types. Single-cell localization trajectories were thresholded, with values below threshold set to the mean intensity of the trace to avoid spurious correlations from low-amplitude fluctuations in the absence of bursting. The autocorrelation function was computed from the thresholded traces and provided an unbiased estimate of the size of the isolated bursts and clusters, which correspond to the two time scale of the exponential decay in the fit (Fig. 2d). The relative frequencies of the two types of bursts can be estimated from the relative weights of the two exponential components of the autocorrelation function (Fig 2d). At concentrations of calcium below 100mM, the average correlation function can be well-described by a single exponential, while at higher calcium levels, two exponentials are needed. In the latter case, the faster of the two timescales matched that obtained in the single exponential fit at low $[Ca^{2+}]$, suggesting that this time-scale corresponds to that of individual bursts. The slower time scale at higher $[Ca^{2+}]$ appears to occur when there is an increase in the frequency of the clustered bursts. Both the value of the slow time scale and its relative weight in the bi-exponential fit increase with $[Ca^{2+}]$, indicating that both the frequency and duration of cluster bursts increases with $[Ca^{2+}]$. This does not affect the FliCR model, as the individual localization bursts that make up the clustered bursts retain the same profile across calcium concentrations. Thus the non-zero portion of the $[Crz1]_{nuc}$ histogram remains the same shape, satisfying Eq. 5, below.

Amplitude variation. In addition to the variability in burst durations, we also found variability in burst heights within a single cell. This variability is unlikely to be due to imaging differences between cells, such as fluctuations in the position of the nucleus with respect to the imaging plane of the microscope because there is little variability in peak intensity of the initial burst. This is usually one of the strongest localization events in a trajectory, but would be expected to exhibit similar amplitude variability during

the initial response if variation in imaging conditions were responsible for amplitude variations. With the characteristic burst duration of ~120 seconds and an acquisition interval of 15 seconds, sampling is sufficiently frequent to capture burst profiles.

Localization score definition. The localization score is not normalized on a 0 to 1 scale because it is difficult to ascertain when full nuclear localization occurs, which is complicated by cytoplasmic autofluorescence and variability in the expression levels of Crz1-GFP in individual cells. Consequently, for simplicity, localization score is shown as extracted from raw data, without normalization.

Crz1 mutants. As shown in Fig. S8 and discussed in the main text, the localization burst frequency is modulated by Crz1 mutations with different affinities for Calcineurin.[1] GFP-Crz1^{high} exhibits a much higher burst frequency than Crz1-mCherry, while Crz1-mCherry is comparable in burst frequency to a mutant with slightly lower affinity for Calcineurin, GFP-Crz1^{low} (Figure S8 a, b). It seems that GFP-Crz1^{wt} has a slightly higher burst frequency than Crz1^{wt}-mCherry (Fig S8 c,d), but the effect is much weaker than that of the difference between GFP-Crz1^{high} and Crz1^{wt}-mCherry. In all three cases, it is exclusively the frequency of bursts that is affected, and never the burst amplitude. FK506 affected burst dynamics in a manner similar to the calcineurin affinity mutations. Frequency modulation of Crz1 bursts is further supported by results showing that expression from 1x, 2x and 4x CDRE promoters remains proportional (coordinated) with respect to FK506 concentration at 100mM Calcium (Fig S8g).

Cell cycle dependence and daughter cells

To monitor the cell cycle dependence of the Crz1 bursts, we observed Crz1-GFP and Whi5-mCherry, a cell cycle marker, simultaneously As described previously, Whi5 is nuclear localized during late G1 phase and relocalizes again at end of mitosis in both the mother and daughter cells,[2] thus serving as a high resolution cell cycle phase indicator. When we cross-correlated the localization events between Whi5 and Crz1 (Fig. S5), we observed only a weak correlation (<10%) between Whi5 and Crz1 activities, indicating that Crz1 bursts do not occur preferentially at particular points in cell cycle, especially not around the end of mitosis. In addition, we found little correlation (<10%) of the Crz1 bursting events between mother cells and daughter cells, suggesting that after division, Crz1 activity becomes completely independent between the mother and daughter.

FRET measurement of calcium fluctuations

Calcium oscillations have been observed in many mammalian systems, but have not to our knowledge been previously observed in yeast.[4] We measured yellow Cameleon YC2.12,[3,4] developed by R. Tsien and colleagues, and Crz1-mCherry simultaneously in the same cell. We observed both isolated Calcium spikes occurring on the timescale ~20-60 seconds and also more prolonged spike trains (Fig. S6). Using 2-second acquisition intervals, we found that the majority of spikes occur on timescales longer than 30 seconds, indicating that our sampling rate is sufficient to capture most calcium spikes (Fig. S7). Every calcium spike coincides with a Crz1 localization event, but not vice versa. However, due to low signal-to-noise ratio of the FRET reporter, we are unable to determine if low amplitude calcium fluctuations contribute to localization bursting activities. When we looked at the calcium spike dynamics as a function of calcium concentration, we found that the number of calcium spikes per trace does not follow the Crz1 burst frequency curves (Fig. S7c).

Msn2 Bursts

Msn2-GFP exhibits nuclear localization bursts under calcium stress (Fig. S9). After the addition of 200mM [Ca^{2+}], Msn2-GFP localized in a synchronized manner across a population and then exited the nucleus in ~10 minutes. Sustained bursting of Msn2 occurred in a manner similar to Crz1. The burst statistics of Msn2 (Fig. S9) shows that the nuclear residence time of Msn2-GFP is approximately 1-2 minutes, similar to that of Crz1. Furthermore, Msn2 also exhibits clustered bursts. However, other than the initial burst in response to calcium addition, the localization events were only weakly correlated between Msn2 and Crz1. As Msn2 bursts occur more frequently under calcium stress than those of Crz1, for each Msn2 burst, there is an 18.4±2.0% chance there is a Crz1 burst occurring at the same time, whereas for each Crz1 burst, there is a 29.7±3.5% chance of coinciding with an Msn2 burst. In contrast, if the two proteins were localized entirely independent, the coincidence probability would have been 14.0±1.2% and 22.6±1.8% respectively (error bar determined by bootstrap). This is consistent with the weak but non-zero cross-correlation between Crz1 and Msn2, showing that while two types of bursts are predominantly independent of each other, there is a statistically significant correlation. Note that Crz1 initial localization were observed at 750mM, but not at 300mM of NaCl. Under these conditions, Msn2 shuttles in and out of the nucleus, indicating that Msn2 is also capable of nuclear localization bursts without being driven by calcium spikes.

Cmk2 in Crz1Δ strain

Cmk2-Venus does not induce in the presence of extracellular calcium in a Crz1Δ strain. The lack of induction is consistent with previous microarray results, where Cmk2 and other Crz1 target genes were not induced in the presence of the calcineurin inhibitor FK506.[6,7] We repeated this experiment at the single-cell level to select appropriate target genes (See below). The Cmk2 FK506 data is specifically plotted in Fig S15a.

Crz1 Localization, Target Promoter Cross Correlation Analysis

The cross-correlation between Cmk2-Venus production rate and Crz1-localization trajectories shows a positive correlation with a peak amplitude of 0.2 and a time-delay of 15 minutes corresponding to the maturation time of the Venus fluorophore. This does *not* mean that only 20% of transcriptional noise is due to localization dynamics. Consider a scenario in which maturation time profile is a square pulse lasting 10 times longer than the localization bursts. Assuming the localization bursts are essentially delta functions, the cross-correlation follows the same profile as the maturation time profile. However, the peak amplitude of the correlation is not 1. By definition, the cross-correlation is normalized by the standard deviation of each component. Consequently, the correlation amplitude is the square root of the duration of the maturation, $1/\sqrt{10}$. Thus, the 0.2 cross-correlation between the Cmk2 promoter activity and Crz1 localization trace should be re-normalized by the maturation time distribution, resulting in a higher correlation coefficient (>50%) between the two dynamic variables. Incomplete correlation could also result from the observation that not all Crz1 localization bursts result in corresponding transcriptional bursts (Fig. S11). The probabilistic nature of transcriptional initiation would further lower the correlation amplitude, again by the square root of the average number of Crz1 localization bursts that occur per expression event.

Maturation time of the Venus fluorophore.

We measured the maturation time of the Venus fluorophore at 30°C on a spectrophotometer (TPI). A 2 ml culture of Hsp12-Venus yeast cells in SC media was induced with 400mM NaCl for 7 minutes and cycloheximide (Sigma) was added to a final concentration of 100 ug/ml to stop translation. Fluorescence traces are shown in Fig. S12. Maturation time was calculated from the derivative of the fluorescence trace, starting from the point of cycloheximide addition, producing a mean value of 15 min.

Fluctuation-Induced Coordinate Regulation (FliCR)

Consider two Crz1 target promoters, A and B, whose normalized rates of expression are Hill functions of nuclear Crz1 concentration, denoted x:

$$R_i(x) = \frac{x^{n_i}}{x^{n_i} + K_i^{n_i}}. \quad (1)$$

Each promoter is thus characterized by half-maximal activation level K_i and Hill coefficient n_i ($i = A$ or B). Here we show that in the FliCR model, the mean promoter expression levels, P_i, are regulated proportionally: $P_A = kP_B$, where k is a constant, at all calcium levels, regardless of K_i and n_i. In the AM model, on the other hand, P_A and P_B in general depend differently on calcium concentration.

To proceed, consider the histogram of x at different calcium levels, $h(x, \mathrm{Ca})$ (Fig. 4). In the AM model, the center of the histogram varies with calcium concentration. In the FM model, on the other hand, the histogram has two components: a peak at high x due to bursts, and a region at low x in the resting state between bursts. Only the relative amplitude of the two peaks, but not their positions, varies with calcium. More generally, if the histogram is not bimodal, it is only important that the shape of the nuclear localization histogram remain the same while its amplitude change relative to the "off" cytoplasmic state. We assume that only the higher peak contributes to expression. As a result,

$$h_{FM}(x, Ca) = f(Ca)g(x), \quad (2)$$

where $f(Ca)$ is the burst frequency as a function of extracellular calcium, and $g(x)$ is the histogram during bursts.

The mean expression level depends on the product, or overlap, between the rate of expression and the histogram of nuclear Crz1 (Box Fig. 1c,d):

$$\overline{P_i(\mathrm{Ca})} = \int R_i(x) h(x, \mathrm{Ca}) dx. \quad (3)$$

In AM regulation, the expression ratio of the two promoters, denoted r_{AM}, may depend in a different way on calcium and hence their ratio is calcium-dependent:

$$r_{AM} = \frac{P_A(Ca)}{P_B(Ca)} = \frac{\int R_A(x) h_{AM}(x,\mathrm{Ca}) dx}{\int R_B(x) h_{AM}(x,\mathrm{Ca}) dx} \quad (4)$$

In FM regulation, on the other hand, the calcium-dependence appears only in the burst frequency, and factors out of the expression ratio, producing a constant expression ratio, r_{FM}:

$$r_{FM} = \frac{f(Ca)\int R_A(x) g(x) dx}{f(Ca)\int R_B(x) g(x) dx} = \mathrm{const.} \quad (5)$$

The result is easiest to see in the extreme limit, when $Crz1_{nuc}$ saturates both target promoters during each localization burst ($x \gg K_A, K_B$). In this case, P_A and P_B are each proportional to the fraction of time Crz1 spends in the nucleus, and hence proportional to each other and to the frequency, f, of Crz1 bursts. Hence their expression ratio P_A/P_B remains fixed as extracellular calcium varies.

Frequency modulation of Crz1 bursts is not the only mechanism to ensure coordinate regulation of downstream targets. FliCR requires the shape of the localization histogram be independent of calcium (Eq. 2), but this could be achieved, for example, by varying the duration of localization bursts, rather than the frequency, similar to Pulse Width Modulation in engineering. Furthermore, the clustering of bursts does not affect FliCR, as the cluster is simply an aggregate of individual bursts. Finally, we note that the argument does not depend on the Hill function itself, and FliCR can work for more complex promoter response functions.

Flow Cytometry Selection Criterion.

Of 163 genes previously shown to be Crz1-dependent[6], 83 had GFP-fusions available.[8] Of these, 19 were excluded because of low induced dynamic range and the resulting difficulty of distinguishing calcium-dependent induction from cellular autofluorescence. We tested the Crz1-dependence of the remaining genes by comparing their response to high concentrations of extracellular calcium with and without FK506, a calcineurin inhibitor (Fig S15). The induction of 40 genes was completely suppressed by FK506, suggesting their expression is predominantly controlled by Crz1. We measured the expression level of each of these 40 genes under 8 concentrations of extracellular calcium (0, 25, 50, 100, 150, 200, 300, 400 mM) using flow cytometry. In the main text, we only show traces up to 300mM for consistency with other experiments. We repeated the experiments measuring the calcium induction of these genes on four separate days. The runs with low cell density (<500 cells per run) were discarded. The remaining runs were normalized according to the following procedure: Each induction curve was fit by least squares (Mathematica) to the CDRE induction curve with two free parameters: offset (minimum expression) and gain (induction range). All normalized curves thus extended from 0 at 0mM [Ca^{2+}] to 1 at 400mM [Ca^{2+}]. For each gene, the means and error-bars of the normalized expression levels were computed from replicate experiments on days with sufficient cell counts.

Out of the 40 genes that passed the FK506 test, 34 showed induction (Fig S14a) curves that closely matches those of burst frequency and CDRE dependence on calcium. The remaining six (Fig S14b) showed different induction profiles. Note that other regulatory mechanisms on the target promoter, such as indirect regulation, can interfere with coordination.

We observed 24 genes whose expression under calcium stress was not completely suppressed with FK506 (>10% induction is independent of calcineurin). In general, the induction curves for these genes depart from the Crz1 burst frequency curve (Fig. S14(c)). This is most likely due to contributions that are calcium-dependent, but not Crz1-dependent. Despite this, Crz1 still plays a significant role in the induction of these genes, as reflected in the similarity of some of these induction curves to the CDRE curves. The difference in target gene sets was due to the fact that our FK506 selection criteria were more stringent than that used in the previous microarray study, that had identified the larger set of target genes initially.

Finally, we examined genes that were independent of Crz1 but are induced in the presence calcium. As expected, they showed different induction profiles compared to pure Crz1 target genes (Fig. S18)

Over-expression of Crz1 rules out "fine-tuned" promoter hypothesis

In principle, coordination could be achieved by 'fine-tuning' of promoter input functions: If all target promoters had input functions that were exactly proportional to each other across $Crz1_{nuc}$ levels, then the target genes would be trivially coordinated. This possibility can be ruled out by considering the response of promoters to changes in the total Crz1 concentration in the cell (Fig. S16).

The 1x, 2x and 4x CDRE promoters exhibit different absolute induction values, but maintain the same normalized induction profiles. Given that all three constructs are driven by the same Cyc1 promoter and differ exclusively in the number of CDRE binding sites,[5] it is unlikely that the increase in expression level occurs without changes in the effective affinity of the promoters. To prove that this is indeed the case, we performed the same induction experiment while overexpressing Crz1.[9] $Crz1^{over}$ also exhibited localization bursts in the presence of calcium (Fig S16b). Synthetic promoters induced with the same induction profile at wild-type levels Crz1 and when Crz1 was overexpressed (see below). However, their absolute expression levels differed (Fig. S16). When Crz1 is overexpressed, the histogram of $[Crz1]_{nuc}$ during a burst shifts to a higher level, resulting in higher overall expression from the promoters. If all three synthetic promoters have the same response function to Crz1, then the induction ratios between the $Crz1^{over}$ and $Crz1^{wt}$ would be identical for all three constructs. However, if the response functions differ among the promoters, the fold change of the overlaps between the $Crz1_{nuc}$ histogram and the response function would be different for the different promoters in overexpressed vs. wild-type Crz1 abundances. This is what we observe experimentally (Fig S16 c,d,e,f): different synthetic promoters depend differently on total Crz1 concentration. The observed induction is 7-fold for 1x and 2 fold for 4x promoters.

Furthermore, note that the larger fold change observed for the 1x promoter may be explained by the following argument. Since the 1x CDRE promoter presumably has a lower affinity to Crz1 than the 4x promoter, the input function for the 1x promoter saturates at a higher concentration of Crz1 than the 4x function. As a result, the wild-type concentration of Crz1 may already be close to saturating the 4x promoter, but not for the 1x promoter, possibly accounting for the larger fold of induction of the 1x promoter.

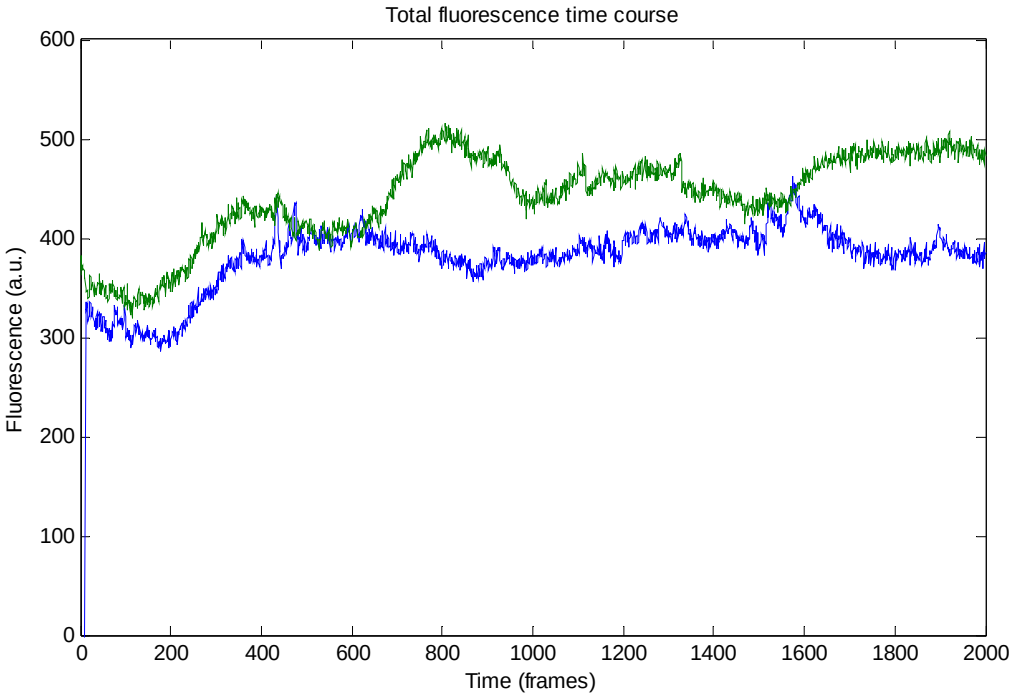

Figure S1. Total Crz1-GFP fluorescence in two cells over the course of a 6 hour movie. 150mM Calcium was added at frame 20. Interval between each frame is 10 seconds.

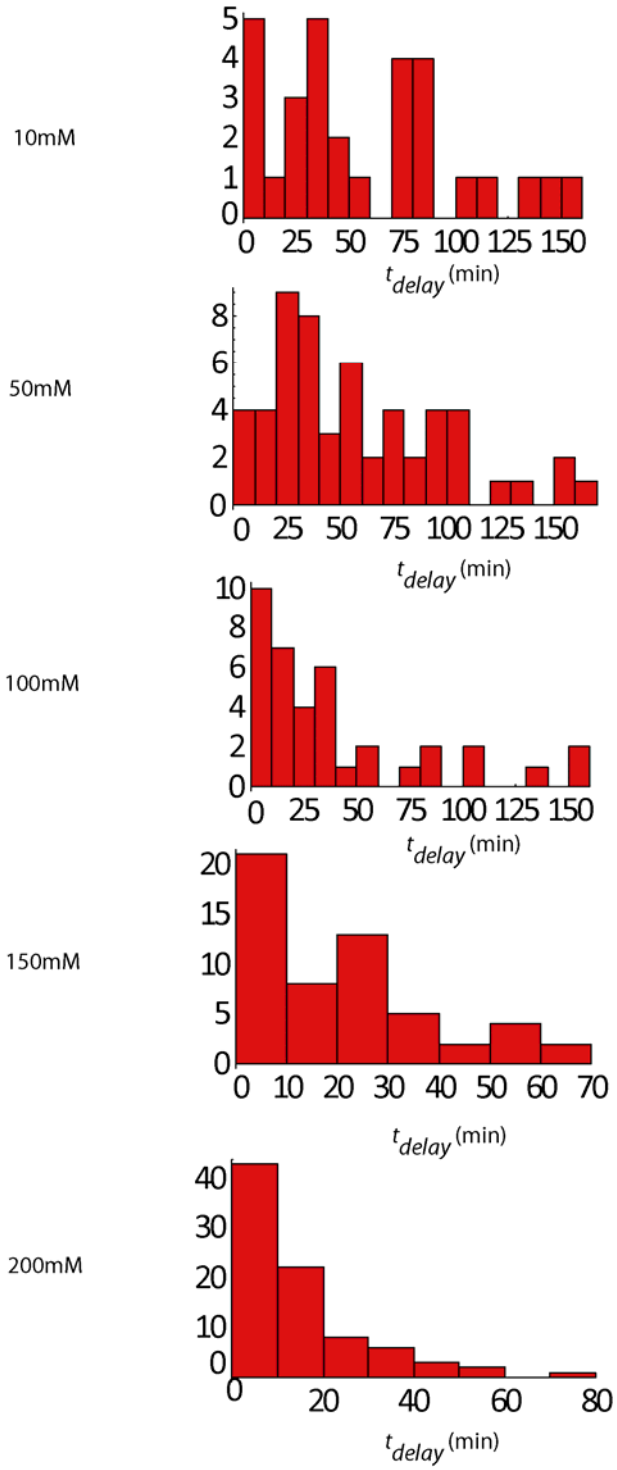

Figure S2. Histogram of delay times between addition of calcium and the initial Crz1 localization burst, τ_{delay}.

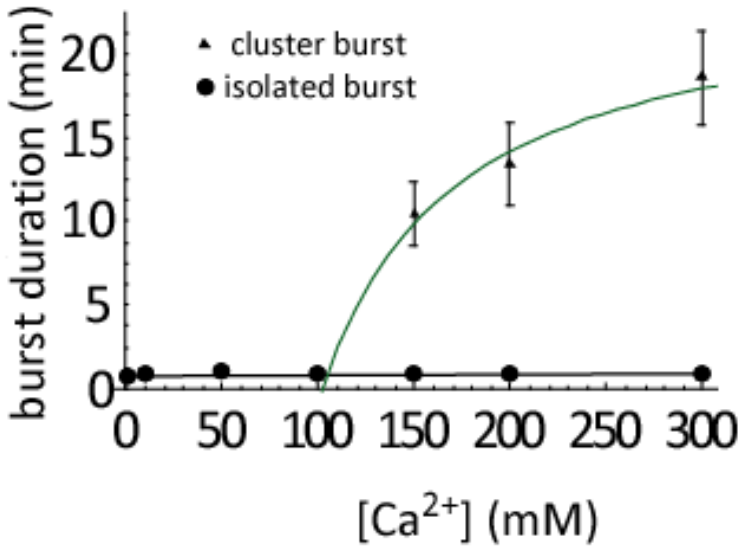

Figure S3. Timescales, τ_{burst} and $\tau_{cluster}$, of isolated (black), and clustered (green), bursts, respectively, at varying calcium concentration. Values were determined by a fit of the autocorrelation function to $A_1 e^{-\left(\frac{t}{\tau_{burst}}\right)} + A_2 e^{-\left(\frac{t}{\tau_{cluster}}\right)}$. Error bars represent sampling errors and were calculated using bootstrap.

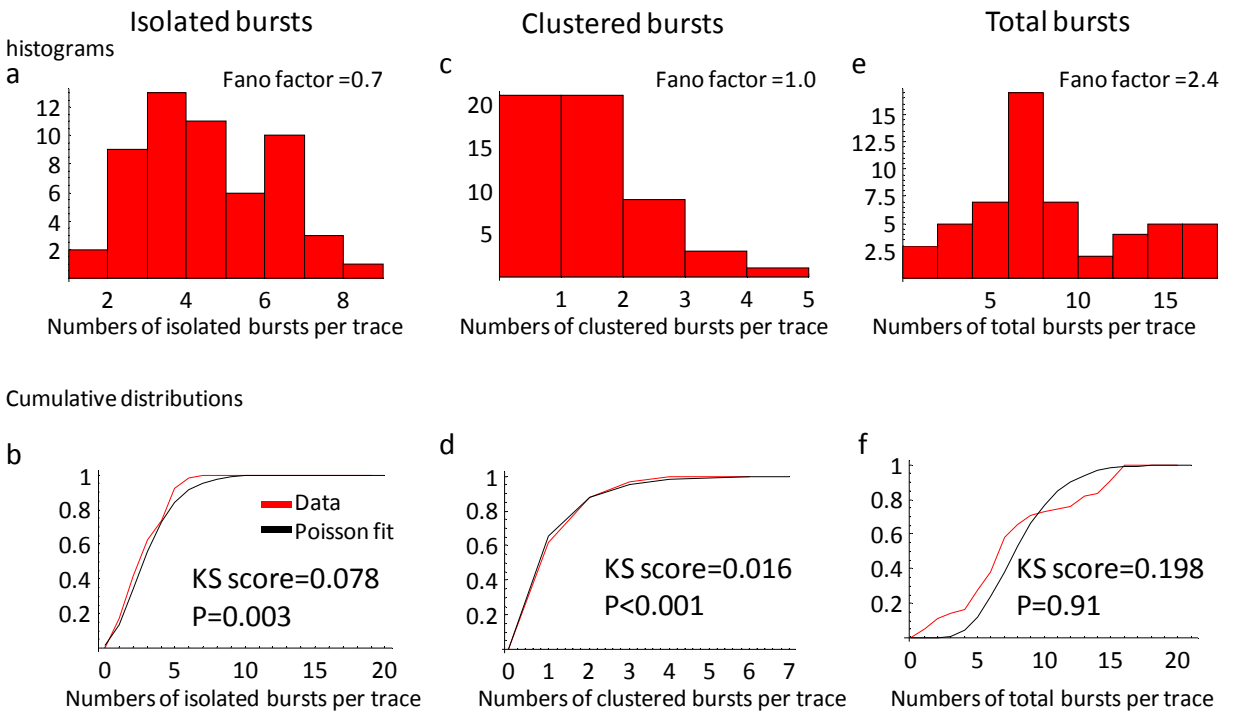

Figure S4. Distributions of number of bursts per trace. Histograms and cumulative distributions of numbers of bursts from a Crz1-GFP movie at 150mM Calcium. Total number of burst per trace is not well-fit by a Poisson distribution, but the numbers of isolated and clustered bursts each fits well to Poisson distribution. Fano factor is the ratio between the variance and the mean of the distribution. The statistics is determined by the Kolmogorov-Smirnov test with the null hypothesis that the data distribution and Poisson distribution are dissimilar.

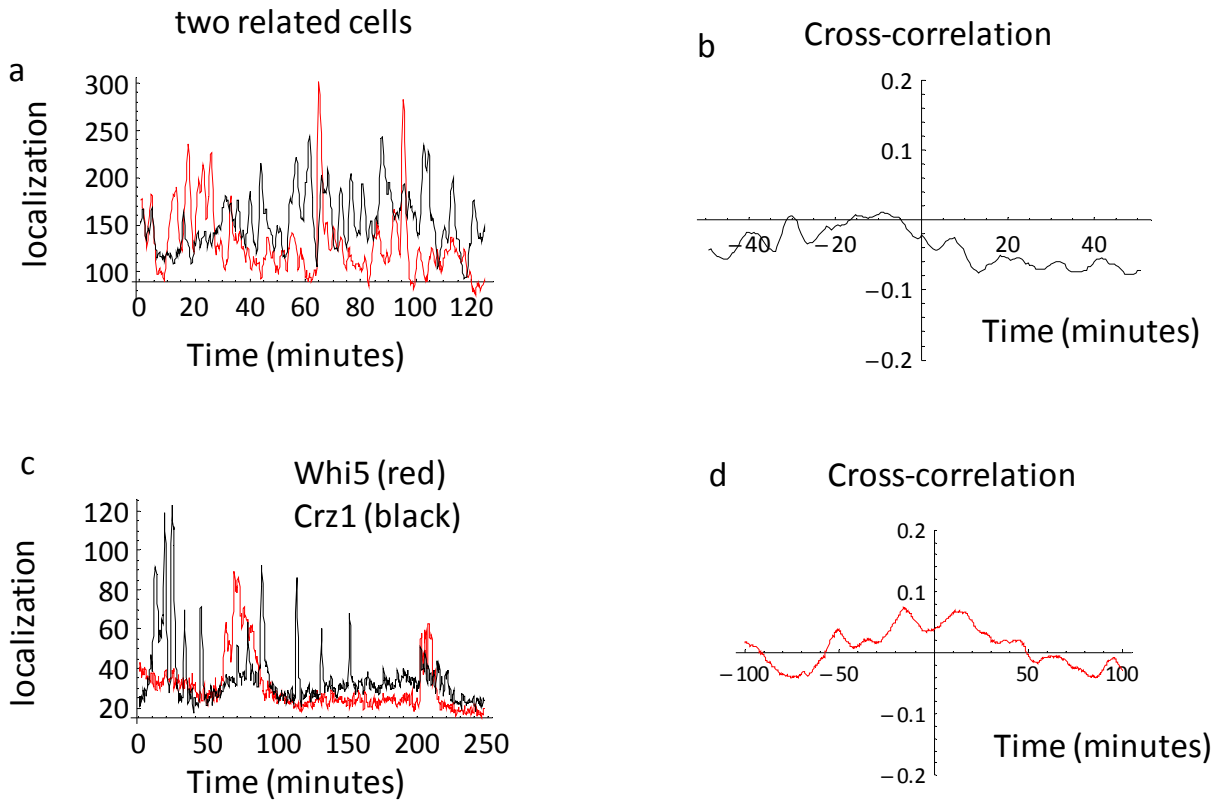

Figure S5. Cell cycle and daughter cell analysis. **a.** A time-trace of a mother cell and daughter cell (black and red) and their **(b)** cross-correlation. **c.** A time-trace of a cell containing cell cycle reporter Whi5-GFP (red) and Crz1-mCherry (black) and their **(d)** cross-correlation.

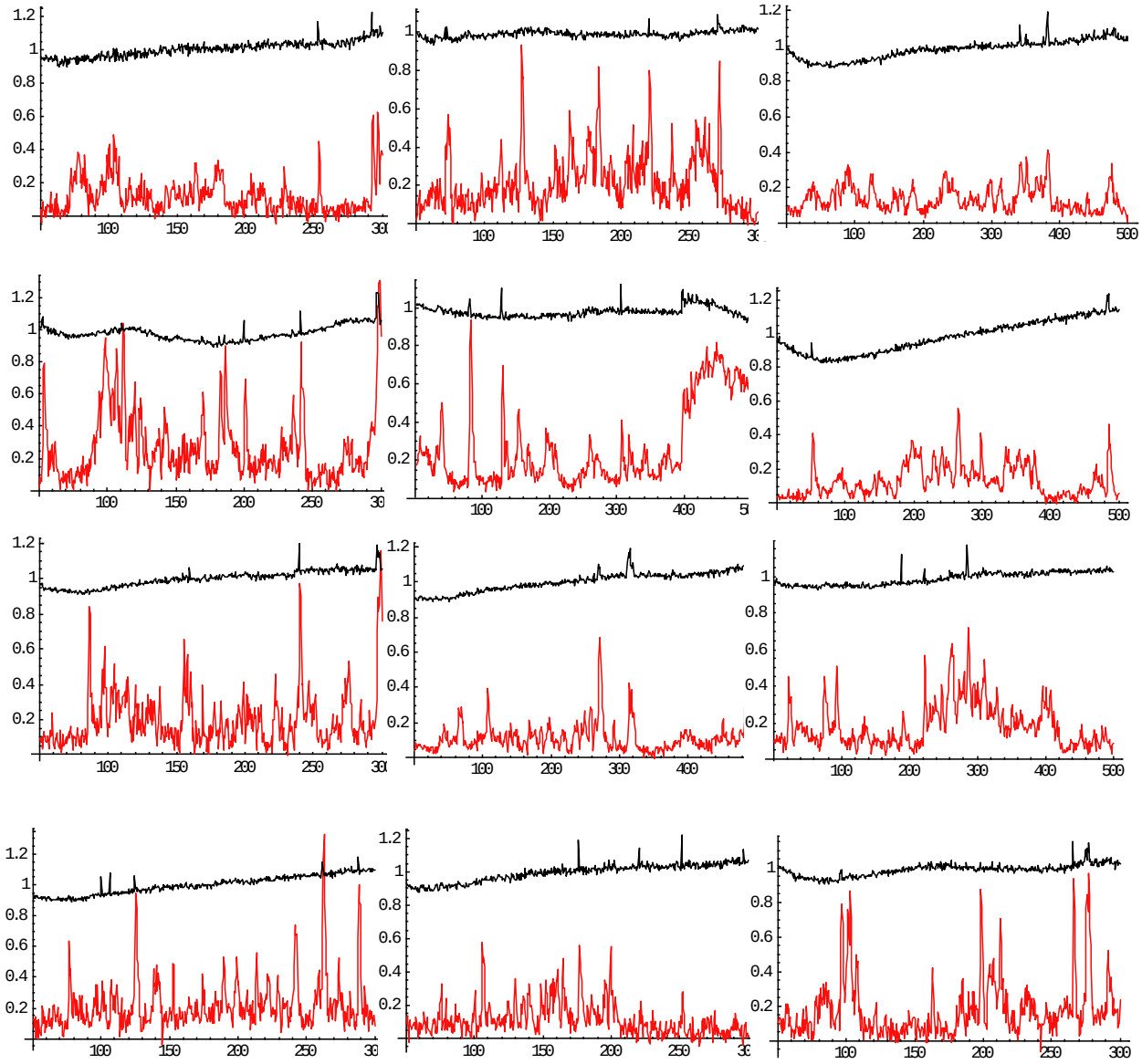

Figure S6. Crz1 localization (red) and FRET ratio (black) traces in single cells at 200 mM extracellular Ca^{2+}. Time is on the x-axis in frames, separated by 30 seconds.

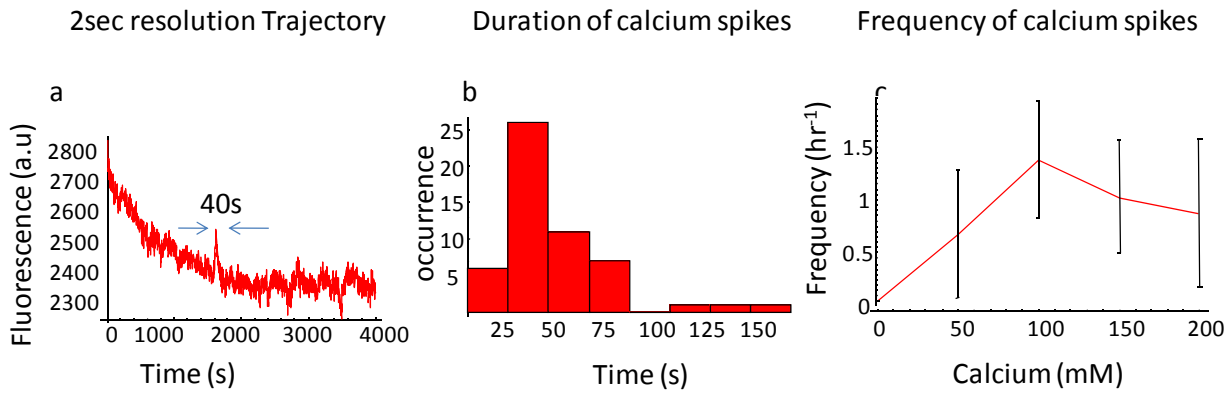

Figure S7. **a.** Typical FRET trace acquired with a 2 sec frame rate showing a calcium spike of ~40 second duration. **b.** Distribution of calcium spike durations from movies like the one shown in (a). Note that mean duration is ~38 sec, and the distribution is peaked around this value. **c**, Frequency of calcium spikes as a function of extracellular calcium concentration. y-axis units are number of spikes per hour. Error bars denotes standard deviation in the number of bursts in one trace.

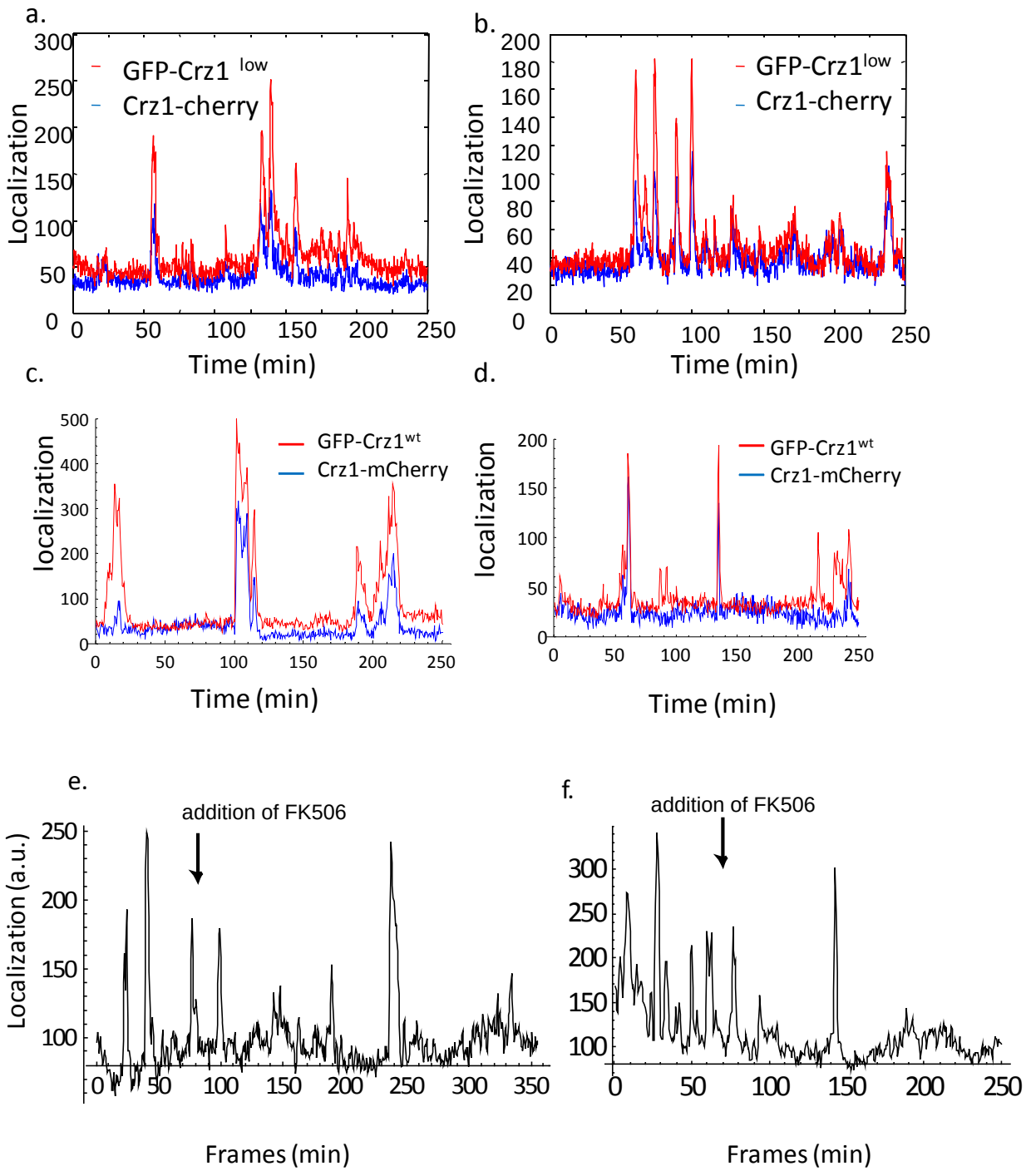
a.
GFP-Crz1 low
Crz1-cherry
Localization
Time (min)
b.
GFP-Crz1low
Crz1-cherry
Localization
Time (min)
c.
GFP-Crz1wt
Crz1-mCherry
localization
Time (min)
d.
GFP-Crz1wt
Crz1-mCherry
localization
Time (min)
e.
addition of FK506
Localization (a.u.)
Frames (min)
f.
addition of FK506
Frames (min)

g

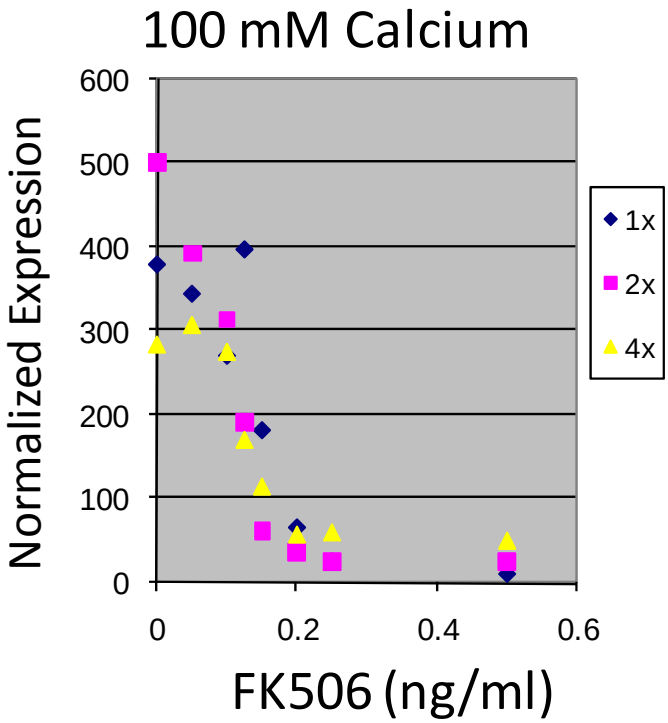

Figure S8. **a,b** Sample traces of Crz1-mCherry and GFP-Crz1^{low} in the same cell. Note that the amplitude differences between the two colors are due to differing fluorophore brightness. **c,d,** Sample traces of Crz1-mCherry and GFP-Crz1^{wt} in the same cell **e,f,** Sample traces of calcium-induced Crz1-GFP after the addition of sub-saturating amounts of FK506. Note that spikes of similar amplitude and duration still occur. **g**, Flow cytometry analysis of the three synthetic promoters induced with 100 mM Calcium and varying amounts of FK506. Note that the three curves collapse onto each other, consistent with frequency-modulation, rather than amplitude modulation, of bursts by FK506.

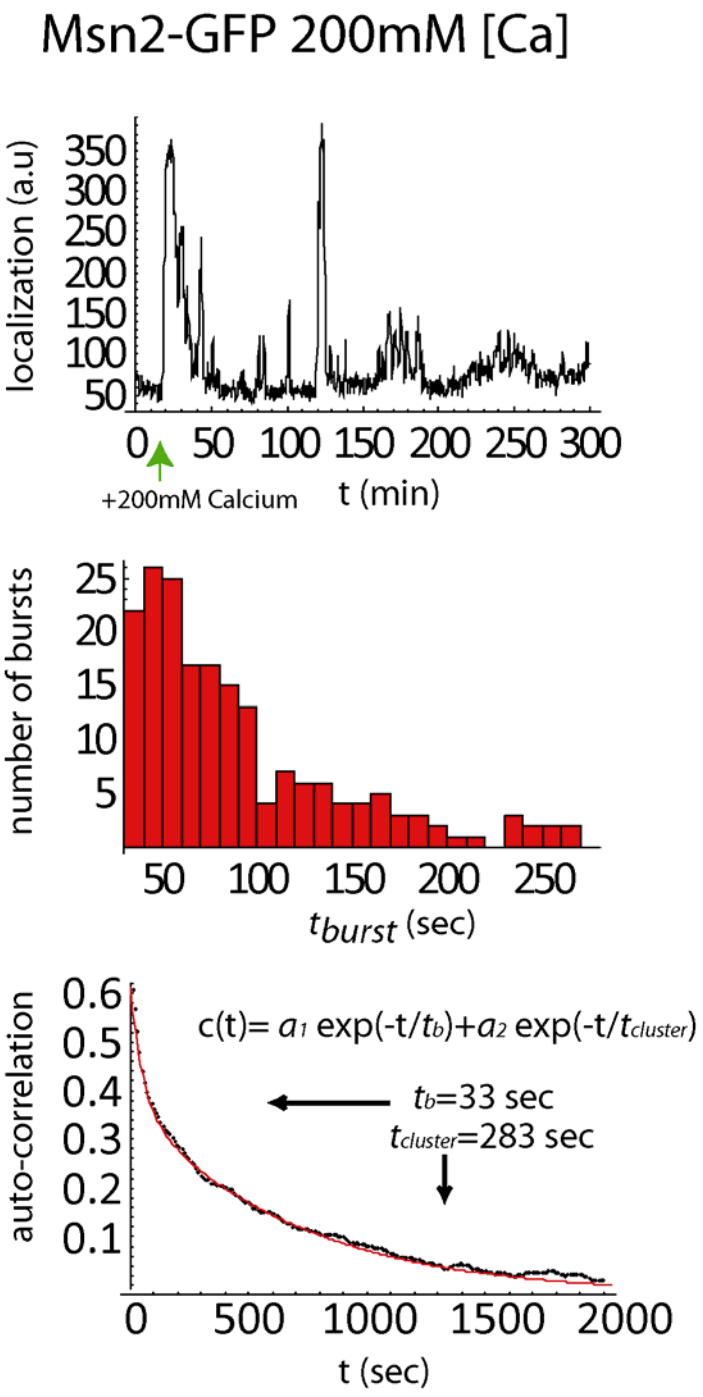

Figure S9. Msn2-GFP bursts in presence of Calcium. The histogram of Msn2 burst duration is similar to that of Crz1, with the majority of bursts lasting between 0.5 to 2 minutes. Autocorrelation shows two timescales of exponential decay representing isolated bursts and clustered bursts. Data is shown in black with two exponential fit shown in red.

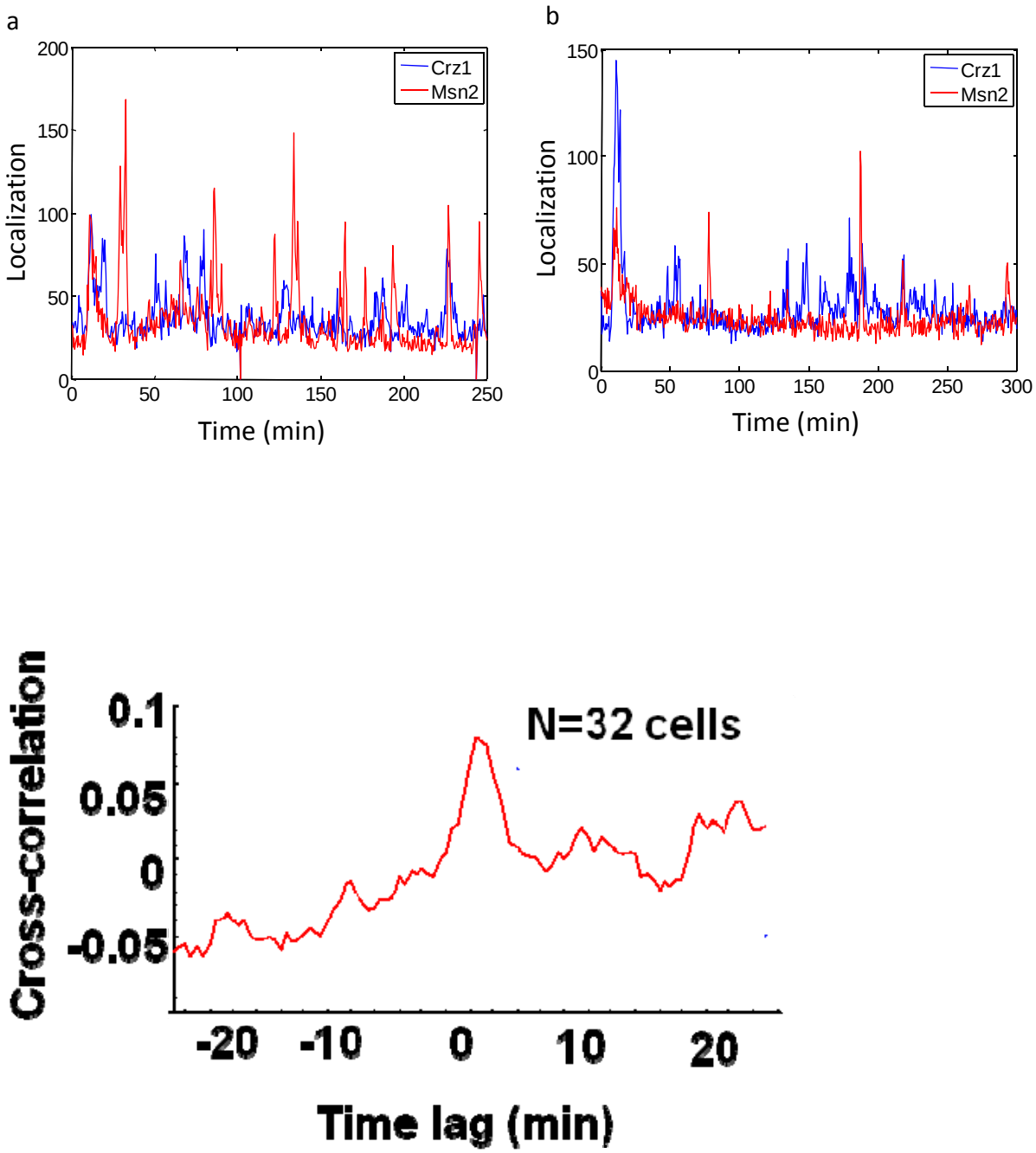

Figure S10. **a,b,** Sample traces of cells containing Msn2-GFP and Crz1-mCherry. **c,** The cross-correlation of Msn2-GFP and Crz1-cherry at 150mM calcium. Note weak correlation (<0.1) peak at 0 time lag.

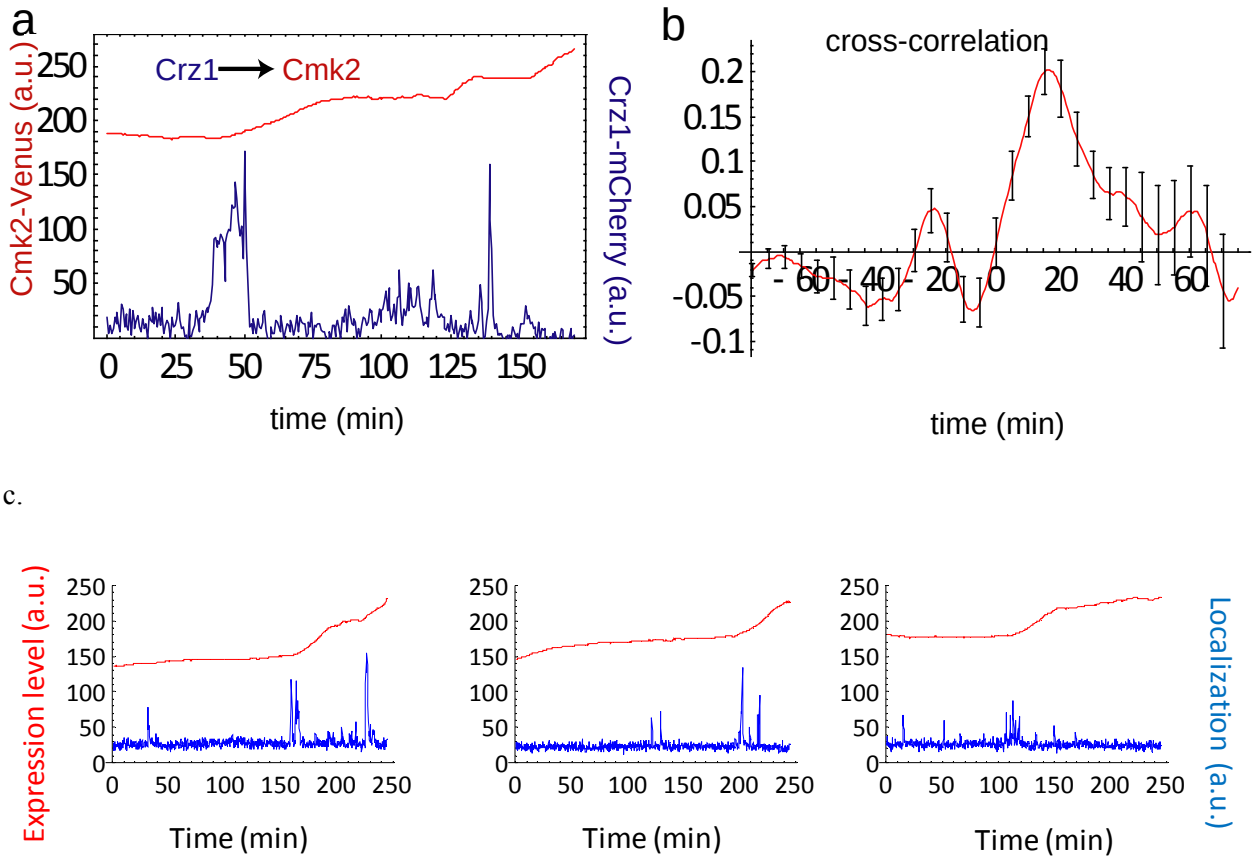

Figure S11. Propagation of Frequency-Modulated localization bursts. **a.** Sample trace of Crz1 localization (blue) and Cmk2 fluorescence (red). **b,** Cross-correlation of Crz1 localization events with Cmk2 expression**. c.** Sample traces of Crz1 localization and 2x CDRE expression.

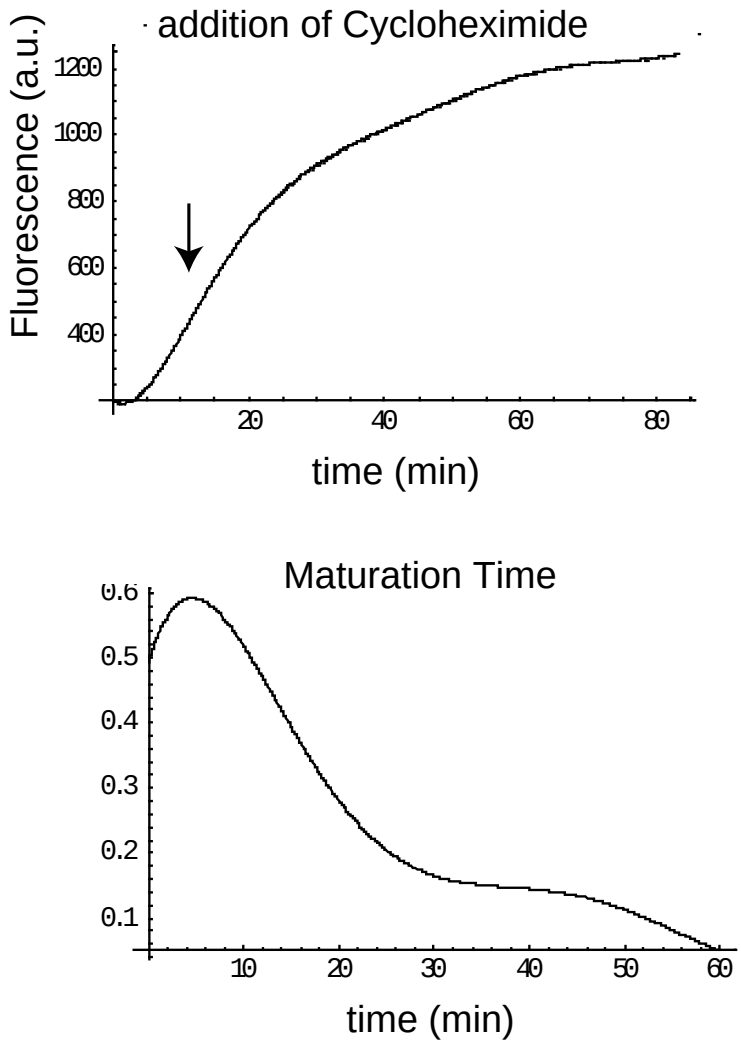

Figure S12. Measurement of maturation time of HSP12-Venus at 30°C. Bottom figure is the time derivative of the top figure, beginning with the time point corresponding to the addition of cycloheximide. A population of cells was measured in a cuvette with a spectrophotometer.

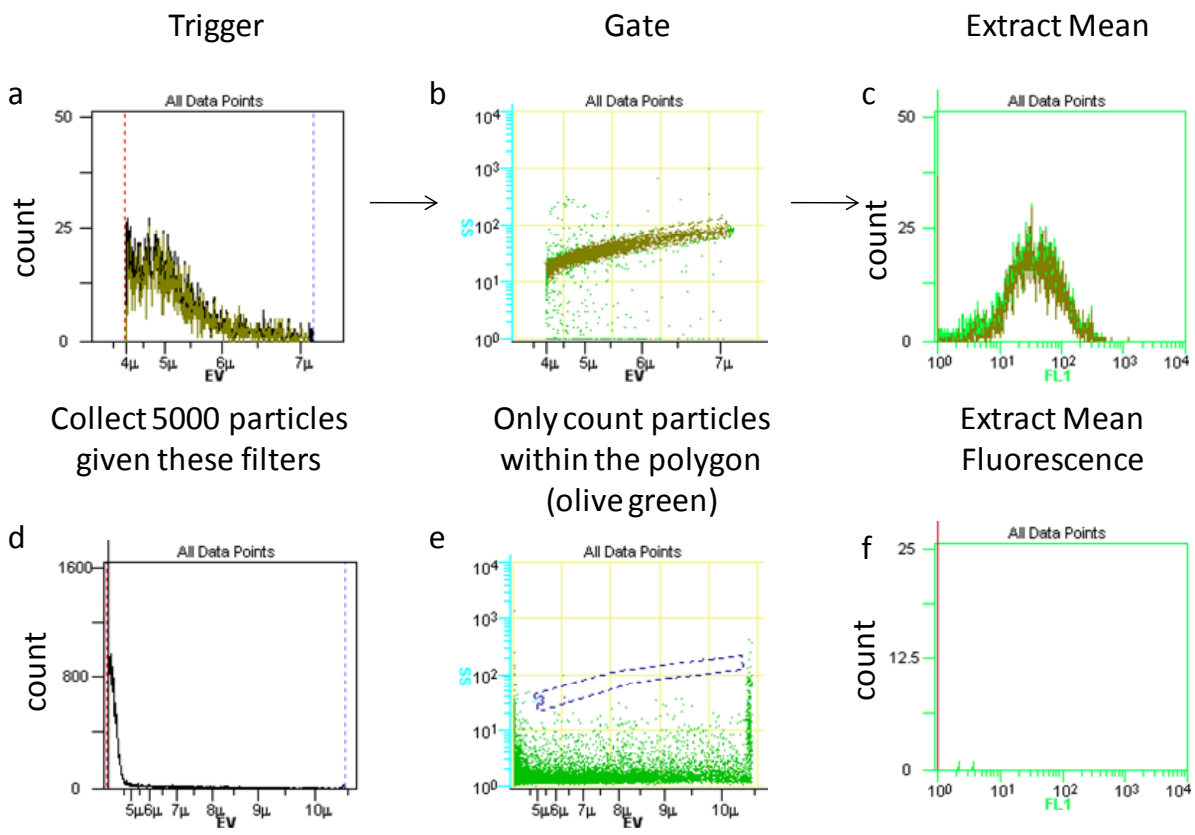

Figure S13. Flow cytometry methods. a-c, Acquisition, trigger and gating of yeast cells on the Beckman Cell Lab Quanta Flow cytometer. EV refers to Coulter volume, or capacitance, measurement of particles. SS refers to side-scatter. **d-f,** Acquisition, trigger and gating of bleach control (no cells).

a.

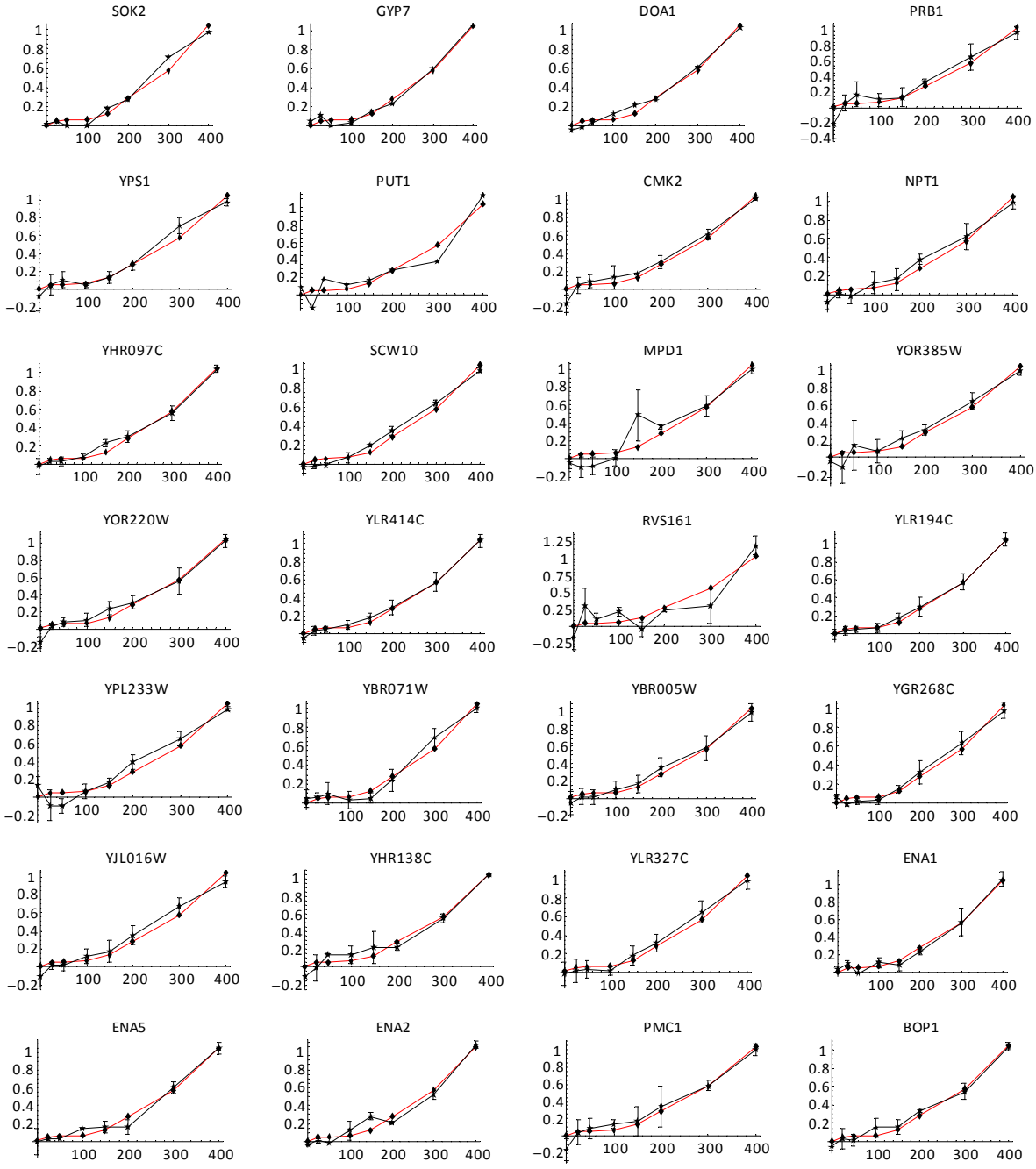
SOK2
GYP7
DOA1
PRB1
YPS1
PUT1
CMK2
NPT1
YHR097C
SCW10
MPD1
YOR385W
YOR220W
YLR414C
RVS161
YLR194C
YPL233W
YBR071W
YBR005W
YGR268C
YJL016W
YHR138C
YLR327C
ENA1
ENA5
ENA2
PMC1
BOP1

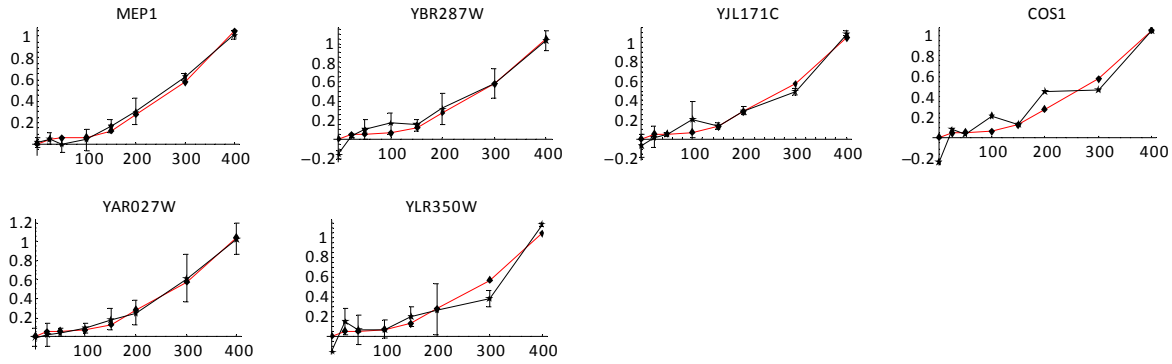

b.

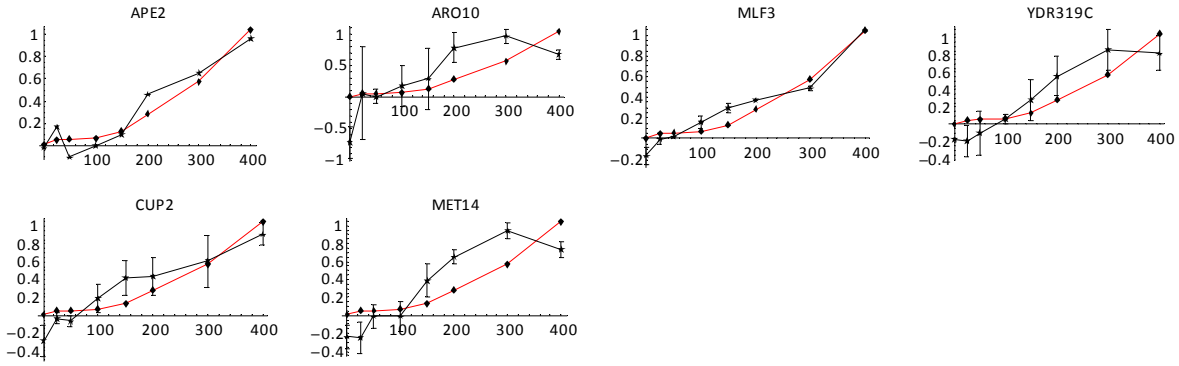

Figure S14 (a,b. 2 pages). Flow cytometry induction curves of Crz1 target genes. Data is plotted in black, with normalized expression levels as a function of calcium concentration, with the fitted synthetic promoter induction curves in red. Error bars are standard errors from repeated measurements. (a) Based on these data, 34 genes fit the synthetic curve very well. (b) APE2, ARO10, MLF3, YDR319C, CUP2, MET14 do not seem to be coordinated, perhaps because of indirect interactions, or errors with our FK506 tests.

c.

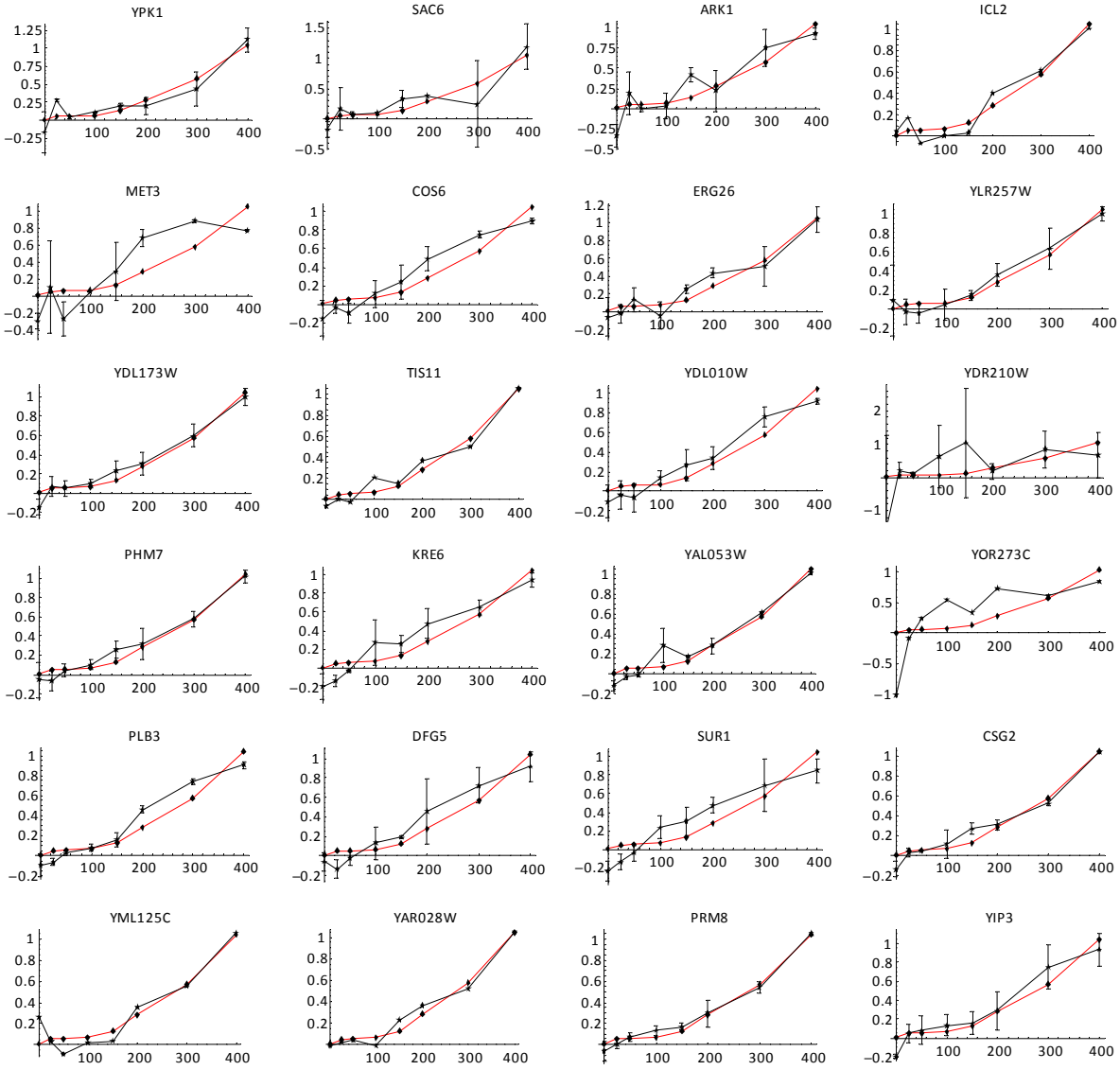

Figure S14 (c). Flow cytometry induction curves of 24 genes that did NOT pass the FK506 test. Note that even though these genes do not pass the stringent FK506-dependence test (Fig. S15), which requires >90% dependence on Crz1, they can still exhibit significant Crz1-dependence, and in fact many of them also fit the CDRE induction curve quite well. For example, in the case of Ark1 (Fig. S15), Calcineurin-dependent activation accounts for >50% of the induction in calcium. Crz1 still contributes a significant fraction of its induction, despite additional contributions to its induction.

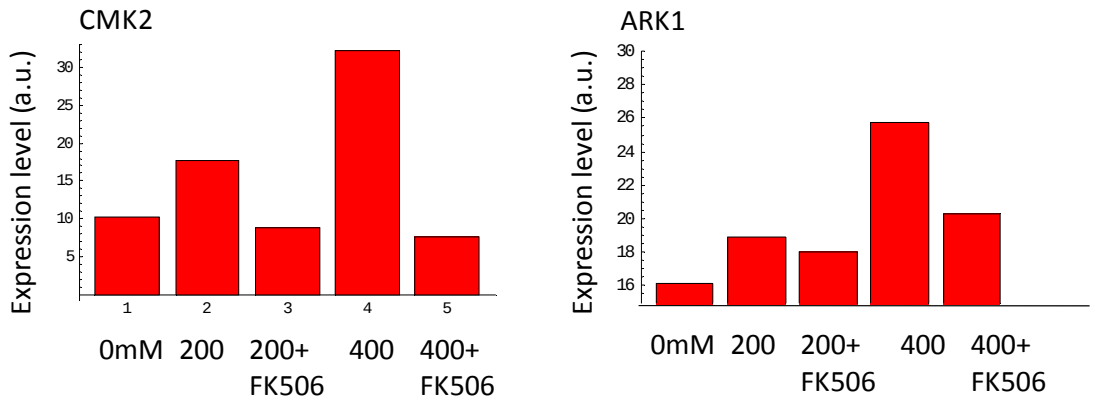

Figure S15. Selection Criterion for target genes. All 83 genes were grown in 0 mM Calcium, 200 mM calcium and 400 mM calcium. Furthermore, cells grown in 200 and 400 mM calcium were also treated with saturating amounts of FK506 (1ng/ml), a calcineurin inhibitor. In the case of Cmk2, negligible induction by calcium is observed in the presence of FK506, indicating that Cmk2 calcium induction is dependent on the Calcineurin/Crz1 pathway. Thus Cmk2 is a target gene that is strongly dependent on Crz1, whereas Ark1 is not: the 400mM Calcium + FK506 data point is not repressed all the way back to basal levels. 24 genes with behavior similar to Ark1 were not considered pure Crz1 targets and were eliminated from the list of target genes.

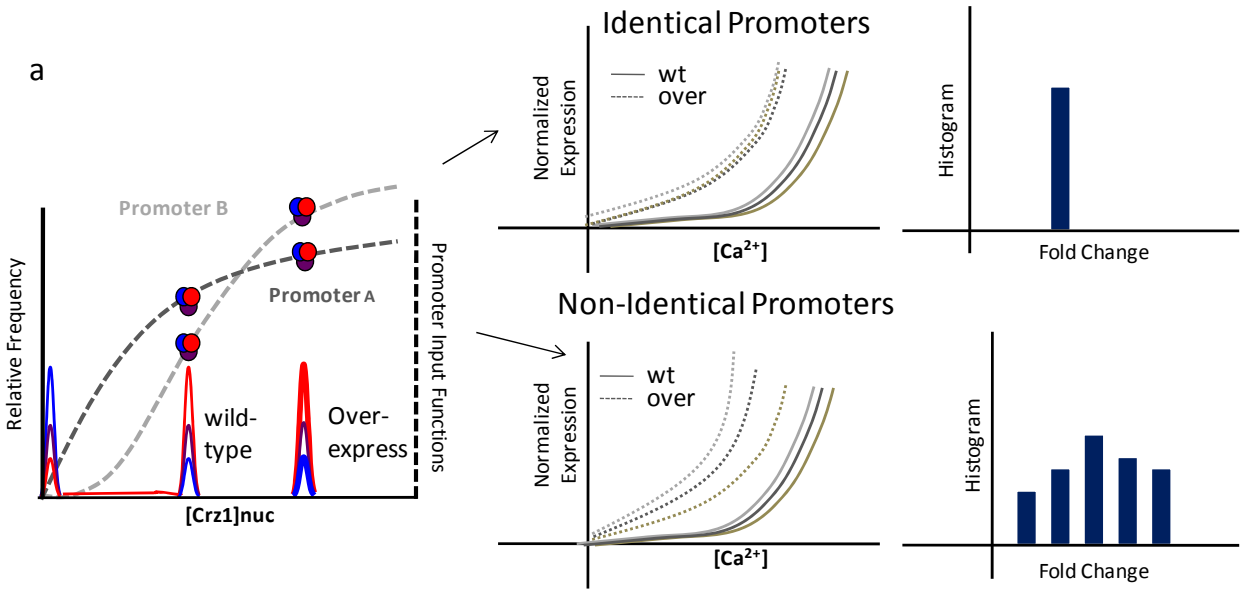
a
Promoter B
Promoter A
Relative Frequency
wild-type
Over-express
[Crz1]nuc
Promoter Input Functions
Identical Promoters
wt
over
Normalized Expression
[Ca2+]
Histogram
Fold Change
Non-Identical Promoters
wt
over
Normalized Expression
[Ca2+]
Histogram
Fold Change

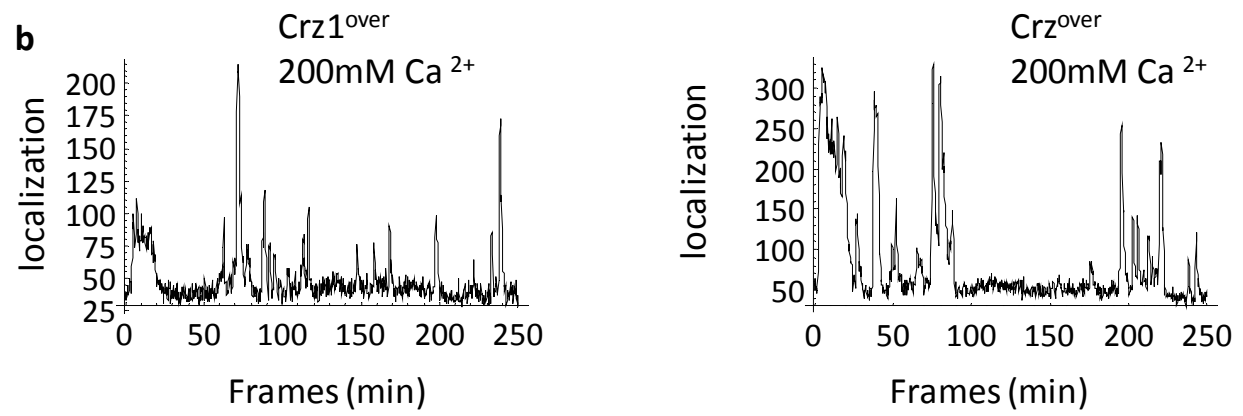
b
Crz1over
200mM Ca 2+
localization
Frames (min)
Crzover
200mM Ca 2+
localization
Frames (min)

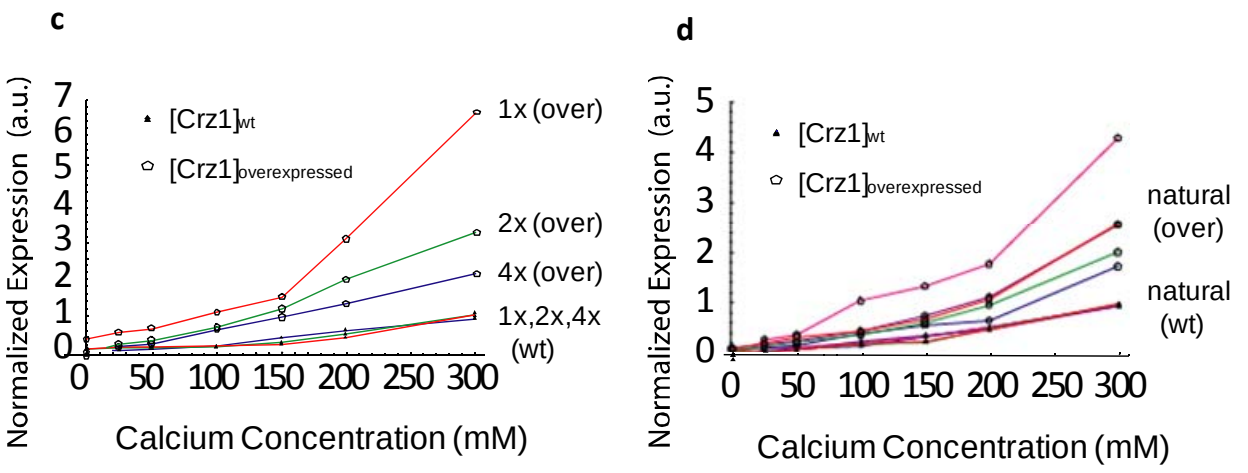
c
[Crz1]wt
[Crz1]overexpressed
1x (over)
2x (over)
4x (over)
1x,2x,4x (wt)
Normalized Expression (a.u.)
Calcium Concentration (mM)
d
[Crz1]wt
[Crz1]overexpressed
natural (over)
natural (wt)
Normalized Expression (a.u.)
Calcium Concentration (mM)

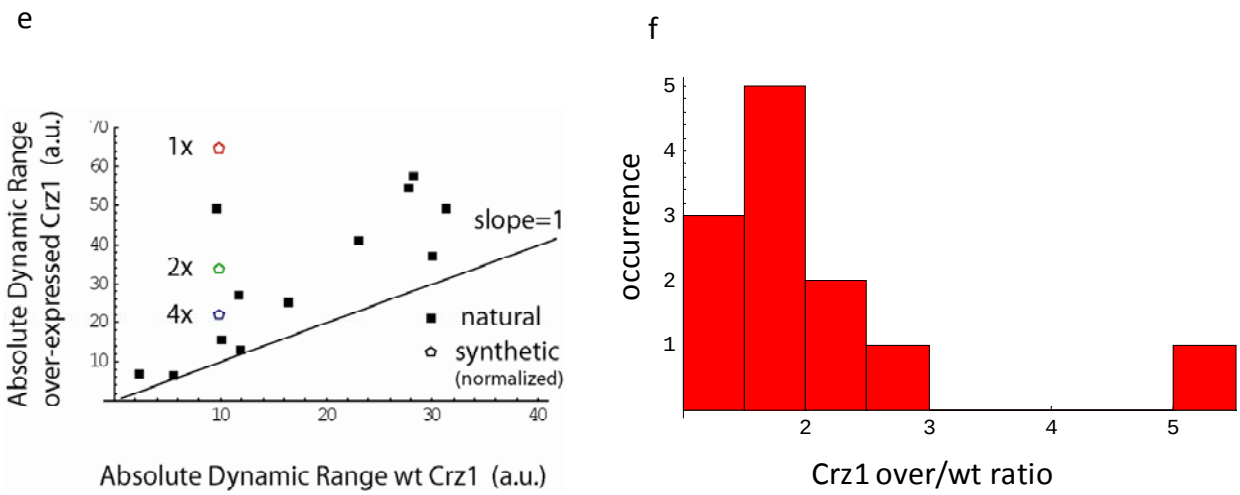

Figure S16. Increasing total Crz1 expression level can exclude identical promoter input functions as an explanation for coordinated regulation. (a) Schematic: Increased total nuclear Crz1 concentrations should cause proportional increases in the expression of promoters with identical input functions, causing them to exhibit identical fold changes between wild-type and overexpressed levels of Crz1. However, if the promoters have different input functions, this fold change should vary, producing the a distribution of fold changes (top right). (b) In a strain that overexpresses Crz1, Crz1-GFP continues to burst as shown in these sample trajectories. (c,d) Expression profiles at wild-type and overexpressed levels of Crz1 for the synthetic and natural promoters. Each promoter activity is normalized by their activity at wild-type Crz1 levels. The diversity of fold changes plotted here shows that target promoters are coordinated despite input function differences (see text). (e) To more clearly see the differences in expression ratio at the two Crz1 levels, we plot the expression level of each promoter. If the promoters had identical input functions the resulting points would all lie on a diagonal line; note instead the scatter in ratios. (f) The histogram of ratio of the absolute dynamic range in overexpression vs. wild-type. If promoters have identical input functions, the histogram would have only a single peak, as illustrated schematically in (a).

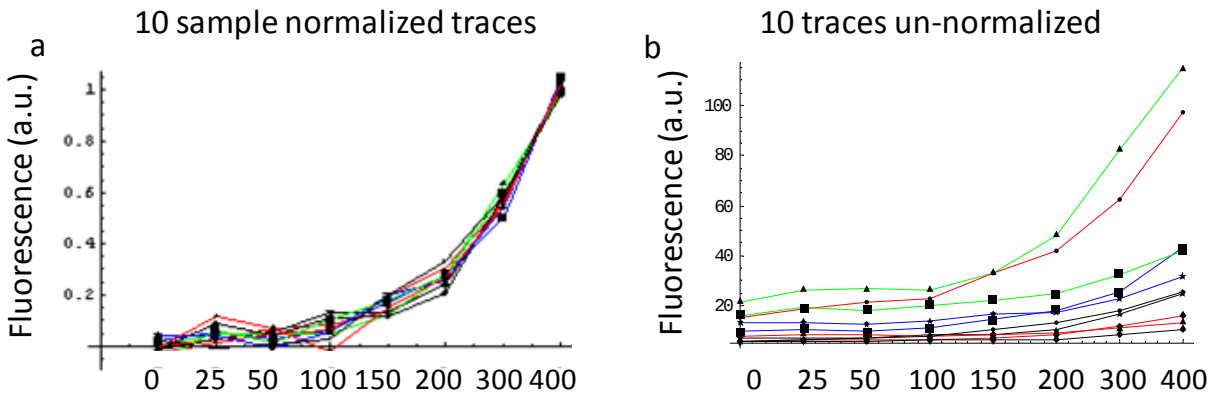

Figure S17. Dynamic range of Crz1 target genes. a, Calcium induction curves, each normalized to its maximum, shown for 10 natural target genes. **b,** The induction curves for the same 10 genes are shown without normalization. Note the range of the absolute expression levels of Crz1 target genes.

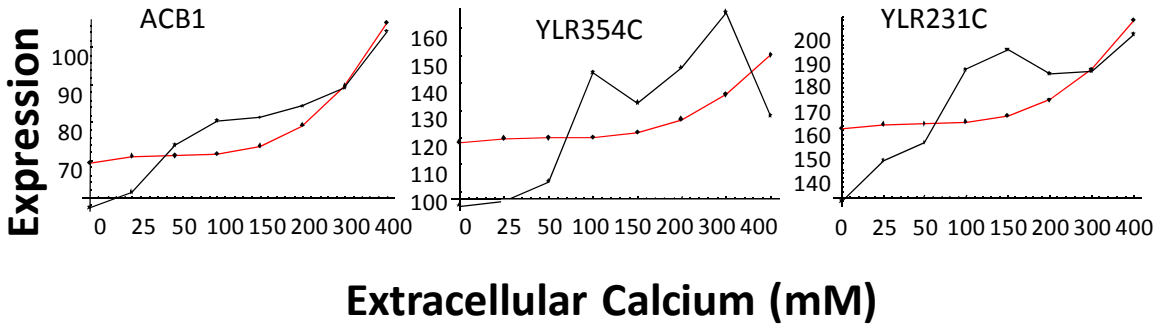

Figure S18. Crz1 non-targets. To ensure that coordinated expression was Crz1-target-specific, we measured the expression of genes which are known to be induced by calcium but not in a Crz1 dependent manner. Their expressions do not match the synthetic CDRE induction curve (red).

References

1 Roy, J., Li, H., Hogan, P. G., and Cyert, M. S., A conserved docking site modulates substrate affinity for calcineurin, signaling output, and in vivo function. *Mol Cell* **25** (6), 889 (2007).

2 Costanzo, M. et al., CDK activity antagonizes Whi5, an inhibitor of G1/S transcription in yeast. *Cell* **117** (7), 899 (2004).

3 Palmer, A. E. and Tsien, R. Y., Measuring calcium signaling using genetically targetable fluorescent indicators. *Nat Protoc* **1** (3), 1057 (2006).

4 Wiesenberger, G. et al., Mg^{2+} deprivation elicits rapid Ca^{2+} uptake and activates Ca^{2+}/calcineurin signaling in Saccharomyces cerevisiae. *Eukaryot Cell* **6** (4), 592 (2007).

5 Stathopoulos, A. M. and Cyert, M. S., Calcineurin acts through the CRZ1/TCN1-encoded transcription factor to regulate gene expression in yeast. *Genes Dev* **11** (24), 3432 (1997).

6 Yoshimoto, H. et al., Genome-wide analysis of gene expression regulated by the calcineurin/Crz1p signaling pathway in Saccharomyces cerevisiae. *J Biol Chem* **277** (34), 31079 (2002).

7 Breuder, T. et al., Calcineurin is essential in cyclosporin A- and FK506-sensitive yeast strains. *Proc Natl Acad Sci U S A* **91** (12), 5372 (1994).

8 Huh, W. K. et al., Global analysis of protein localization in budding yeast. *Nature* **425** (6959), 686 (2003).

9 Matheos, D. P., Kingsbury, T. J., Ahsan, U. S., and Cunningham, K. W., Tcn1p/Crz1p, a calcineurin-dependent transcription factor that differentially regulates gene expression in Saccharomyces cerevisiae. *Genes Dev* **11** (24), 3445 (1997).